

# Surface restoration in hygroscopic $\text{VI}_3$ crystals via synchrotron soft X-ray irradiation

A. De Vita,<sup>\*,†,‡</sup> V. Polewczyk,<sup>¶</sup> G. Panaccione,<sup>§</sup> and G. Vinai<sup>\*,§</sup>

<sup>†</sup>*Institut für Physik und Astronomie,*

*Technische Universität Berlin, Strasse des 17 Juni 135, 10623 Berlin, Germany*

<sup>‡</sup>*Fritz Haber Institute of the Max Planck Society, Faradayweg 4–6, 14195 Berlin, Germany*

<sup>¶</sup>*Université Paris-Saclay, UVSQ, CNRS, GEMaC, 78000, Versailles, France*

<sup>§</sup>*CNR - Istituto Officina dei Materiali (IOM), S.S. 14, km 163.5, 34149 Trieste, Italy*

E-mail: alessandro.de.vita@tu-berlin.de; vinai@iom.cnr.it

## Abstract

Among van der Waals crystals, transition metal trihalide  $\text{VI}_3$  has driven attention for its magnetic and orbital properties. However, its chemical instability under ambient conditions make its exploitation challenging for technological implementation. In this context, here we show how synchrotron radiation soft X-rays partially restore stoichiometric chemical and electronic properties of  $\text{VI}_3$  crystals. By combining X-ray absorption and X-ray photoemission spectroscopies, we show as-cleaved and aged (in ultra-high vacuum conditions) chemical degradation of  $\text{VI}_3$  crystal surface, with the formation of vanadates, and its, at least partial, recovery under high-flux soft X-ray beam exposure, revealing that superficial hygroscopic contamination couples relatively weakly to the crystal surface.

# Introduction

The family of two-dimensional (2D) materials has considerably expanded with the discovery of van der Waals crystals, with major consequences for the landscape of functional materials due to different properties emerging when moving from single crystals to monolayers or heterostructures.<sup>1,2</sup> Among them, triiodides  $XI_3$  ( $X = \text{Cr}, \text{V}$ ) stand out for their long-range magnetic properties and rich temperature-dependent phase diagram, with promising applications in the field of spin- and orbitronics.<sup>3-8</sup> In particular,  $VI_3$  shows ferromagnetism down to monolayer thickness<sup>9</sup> characterized by a reduced spin dimensionality,<sup>10</sup> a spin reorientation transition,<sup>11</sup> and a large orbital magnetic moment at 2 K<sup>12</sup> that gets quenched in proximity of the spin reorientation.<sup>10</sup> Conversely, it has been noted that  $XI_3$  are highly unstable under ambient conditions, making their handling challenging. The instability is mostly driven by reaction to moisture, since  $H_2O$  hydrates the crystal by replacing the  $I^-$  ligands coordinated with the metallic centers. This leads the surface of bulk  $VI_3$  crystals to decompose into droplets, losing their crystallographic and magnetic properties, even in presence of protective oil layers.<sup>13-15</sup> In this sense,  $VI_3$  shares its hygroscopicity with  $CrI_3$ , whose flakes degrade via photocatalytic substitution of iodine by water, a process accelerated by light illumination.<sup>16</sup> A road towards leveraging the hygroscopicity the same way as for more stable sister compounds, such as  $CrCl_3$ ,<sup>17</sup> appears more challenging.

In this context, here we present a synchrotron radiation soft x-ray investigation on the stability in ultra-high vacuum (UHV) conditions of  $VI_3$  crystals upon aging. By combining absorption and photoemission spectroscopic measurement, we show that V  $2p$  edges are mostly affected by moisture, leading to the formation of superficial vanadates. We then show how surface exposure to relatively mild photon fluxes is sufficient to alter the surface bonds of  $VI_3$  with moisture, leading to a partial recovery of the stoichiometric chemical properties.

## Experimental section

**Sample handling** – Commercially available  $\text{VI}_3$  crystals stored in a glovebox filled with Ar atmosphere ( $< 0.5$  ppm of  $\text{O}_2$ ,  $< 0.5$  ppm of  $\text{H}_2\text{O}$ ) have been transferred in inert static atmosphere and cleaved inside the loadlock chamber (base pressure  $< 10^{-8}$  mbar), to expose the (0001) crystallographic plane of the clean surface. The samples were held in high vacuum (pressure  $\sim 5 \times 10^{-9}$  mbar) for 72 hours (aged sample) and measured afterwards. We estimate the exposure of the surface to be  $\sim 2600$  L. A second set of samples was introduced via the same procedure via glovebox, and directly cleaved at the endstation chamber in ultrahigh vacuum (UHV, pressure  $< 3 \times 10^{-10}$  mbar), *i.e.*, in better vacuum conditions ( $\sim 2$  L).

**XAS and XPS characterizations** – X-ray absorption (XAS) and X-ray photoemission spectra (XPS) were carried out at APE-HE beamline of NFFA at the Elettra synchrotron radiation facility in Trieste.<sup>18</sup> The sample surface was kept at  $45^\circ$  with respect to the incident X-rays, for a beam footprint on the sample surface of around  $150 \mu\text{m} \times 150 \mu\text{m}$ . XAS were measured in linear horizontal polarization at room temperature in total electron yield (TEY) mode, normalizing the intensity of sample current to the incident photon flux current at each energy value. The photon flux intensity was modulated by opening or closing mechanical exit slits placed after the spherical mirror, whose intensity is estimated by measuring the TEY signal of a gold-plated W grid placed in front of the endstation, and converting it into photons/s following beamline calibrations in ref.<sup>18</sup> XPS measurements were taken with a ScientaOmicron R3000 analyzer, in horizontal polarization, with a photon energy of 800 eV, with the sample surface normal to the analyzer and at  $45^\circ$  with respect to the X-ray beam.

## Results and discussion

Firstly, we analyze the effects of surface aging in vacuum conditions on a  $\text{VI}_3$  crystal cleaved at room temperature.

Fig. 1a illustrates the survey acquired for the two different surface conditions: as-cleaved

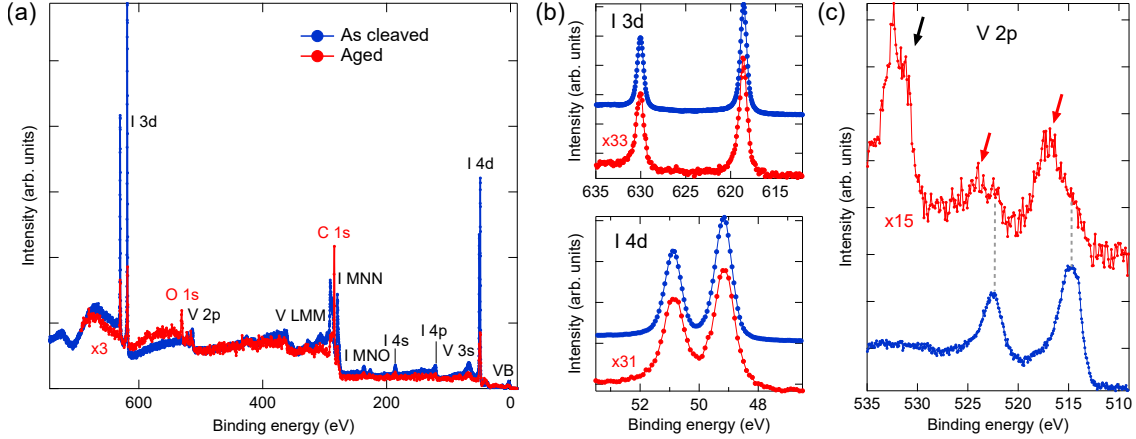


Figure 1: (a) XPS survey at 800 eV on  $\text{VI}_3$  as-cleaved (blue) and aged (red) samples, with element-specific peaks highlighted. (b)  $\text{I } 3d$  and  $4d$  edges for as-cleaved (blue) and aged (red) samples. (c)  $\text{V } 2p$  and  $\text{O } 1s$  edges for as-cleaved (blue) and aged (red) samples. All measurements were done with a photon flux equivalent to  $2.8 \times 10^9 \text{ photons s}^{-1}$  on the mesh.

(blue curve) and aged, *i.e.*, after 72 hours in UHV (red curve). We can see that the intensities of the signals from  $\text{I } 3d$  and  $4d$  edges (Fig. 1b) and  $\text{V } 2p$  edges (Fig. 1c) – the former in particular – are strongly reduced in the aged sample; additionally, strong  $\text{C } 1s$  and  $\text{O } 1s$  peaks appear, suggesting a contaminated surface environment. Further examination of the element-specific photoemission edges give more information on the chemical condition of the surface in the two samples. On one hand the  $\text{I } 3d$  and  $4d$  signals, albeit much less intense, show an effectively unaltered lineshape (Fig. 1b); on the other hand, the  $\text{V } 2p$  doublet displays additional features at higher binding energies (red arrows in Fig. 1c). The above suggests that the chemical environment of vanadium is considerably altered at the surface of  $\text{VI}_3$ , whereas the chemical state of bonded iodine is mostly unchanged. A structured  $\text{O } 1s$  peak (black arrow in Fig. 1c) is also present on the aged sample and hints at a complex chemical state of this element at the surface. Since  $\text{I}$  core levels are not modified by spurious oxygen contamination, we consider the  $\text{O } 1s$  peak as composed by a combination of  $\text{V-O}$  bonds and molecular oxygen, whereas  $\text{V } 2p$  combines stoichiometric  $\text{VI}_3$  features, here almost vanished, with the formation of high-valence vanadates. A more detailed analysis will be given in the following.

To capture more details of the valence state of  $\text{V}$  and further understand the role of the

metallic centres in the chemical modification on the surface, we measured XAS spectra across the V  $L_{2,3}$  edges for both samples. Experimental spectra are shown in Fig. 2. The lineshape of the as-cleaved spectrum follows expectations for a  $V^{3+}$  oxidation state, including all the pre-edge features (1-2) and (7-8) from empty  $t_{2g}$  states.<sup>10,19,20</sup> Conversely, the aged sample presents an overall shift towards higher photon energies, as well as significant differences in lineshape. The main  $L_3$  peak (6) displays a shift of 1.6 eV compared to pristine  $VI_3$  (4) and an overall skew towards high-energy components of the multiplet; the lineshape and bandwidth of the  $L_2$  edge is similarly altered; we also note the absence of well-defined pre-edge states.

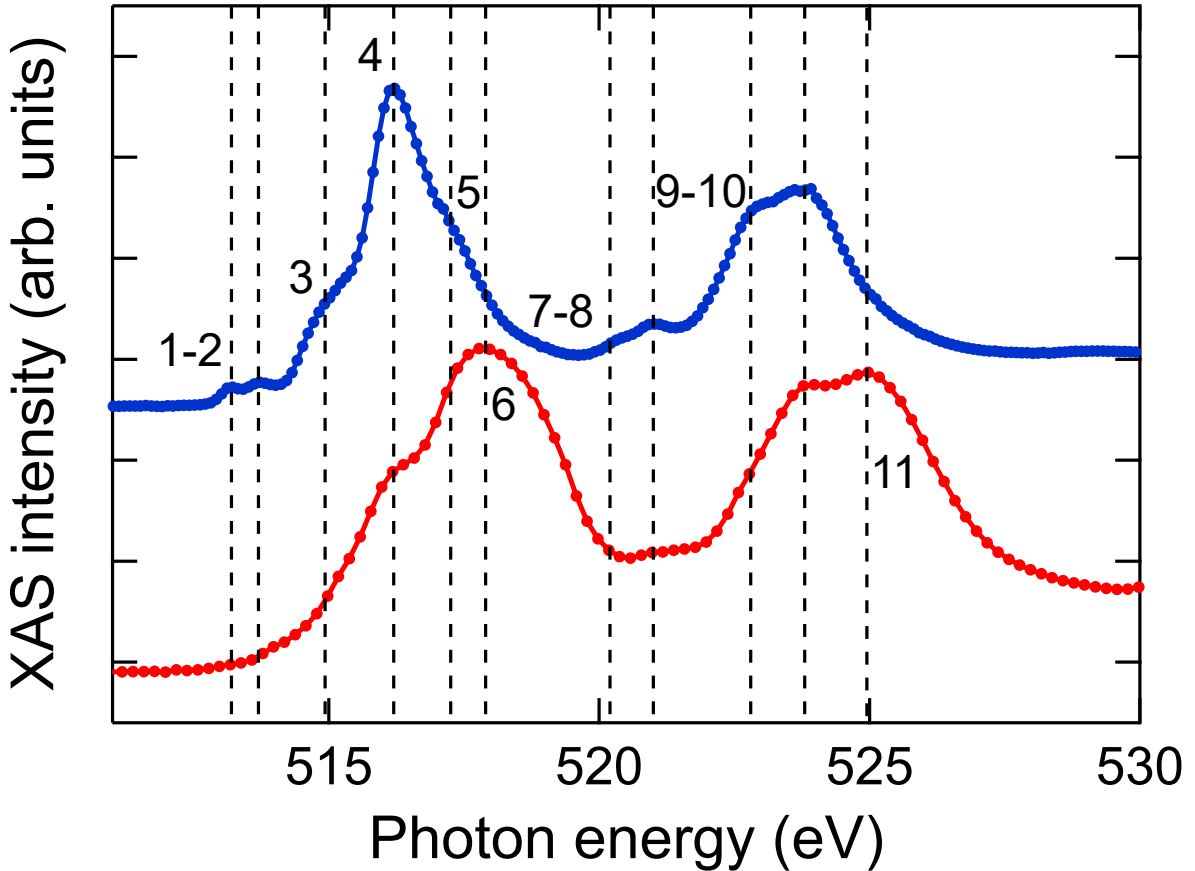


Figure 2: XAS spectra at V  $L_{2,3}$  edges on as-cleaved (blue) and aged (red) samples. The photon flux for these spectra was equivalent to  $2.8 \times 10^9$  photons  $s^{-1}$  at the gold-plated mesh grid before the endstation.

The results suggest a relevant change in the orbital configuration of V upon surface contamination. In particular, the lineshape of the aged sample displays similarities with 4+ and

5+ valence states, by comparison with absorption spectra of vanadates and vanadium oxides.<sup>21–24</sup> It is likely that this modification is significantly affecting more than the first atomic layer, since the probing depth of the technique amounts to 4 nm to 6 nm in the employed photon energy range:<sup>25</sup> this corresponds to around seven unit cells in the monoclinic phase, each composed of a double layer of  $\text{VI}_6$  octahedra (space group  $C2/m$ ,  $c = 6.9502(4) \text{ \AA}$ <sup>26</sup>).

During these XAS measurement, the surface conditions have been monitored by XPS surveys and core level spectra; no significant evolution was observed with all measurements taken for a photon flux  $\approx 0.28 \times 10^{10} \text{ photons s}^{-1}$  on the gold-plated mesh grid (see SI Fig. S1). On the other hand, once the photon flux was increased up to  $\approx 2.40 \times 10^{10} \text{ photons s}^{-1}$ , the lineshape of the XAS spectra changed dramatically, as displayed in Fig. 3a. In particular, we notice a gradual increase of low-energy features of the spectrum, as well as, importantly, the appearance of pre-edge signals. This change is not a transient effect, as decreasing the flux does not result in a recovery of the high-energy features. Conversely, when probing another spot on the sample surface, the previous lineshape is retrieved (SI, Fig. S2). These are indicators of a local effect of soft X-ray irradiation on the exposed area of the crystal, which amounts to a chemical modification of the superficial bonds between the crystal and oxygen contaminants.

In order to quantify the change in the chemical state of V as probed by XAS, we fitted the experimental spectra at different flux intensities with a linear combination of the spectral features ascribed to reference  $\text{V}^{x+}$  spectra, as measured on the same beamline. The reference spectra belong respectively to pristine bulk  $\text{VI}_3$  ( $\text{V}^{3+}$ ),  $\text{VSe}_2$  ( $\text{V}^{4+}$ ), and the over-oxdized surface layer of  $\text{SrVO}_3$  ( $\text{V}^{5+}$ ).<sup>19,27,28</sup> In the case of  $\text{V}^{4+}$  and  $\text{V}^{5+}$  contributions, a broadening has been included to account for the absence of monocrystalline order of these compounds on the  $\text{VI}_3$  surface and the consequent blurring of sharp multiplet peaks. The procedure is performed on a range up to 528 eV, due to the interference of the overlapping O edge especially for the  $\text{V}^{5+}$  component. Our fits succeed in reproducing the main features of the measurements (Fig. 3b-c) and reveal that the main contributions at low flux come from  $\text{V}^{4+}$

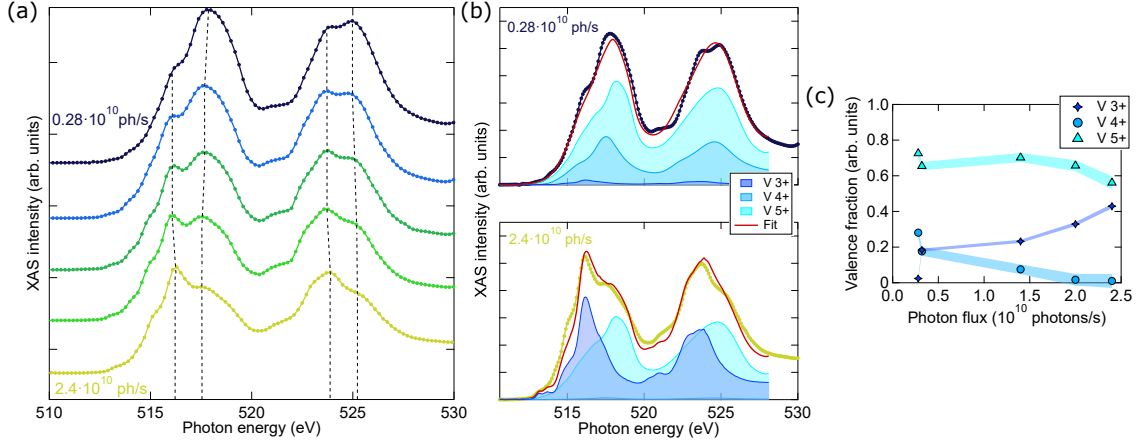


Figure 3: (a) Subsequent XAS spectra at V  $L_{2,3}$  edges on the same probed area, from top to bottom, under increasing photon flux irradiation. (b) Fitted XAS spectra with reference spectra for the first spectrum at low irradiation flux (top black curve) and last measure at high irradiation flux (bottom yellow curve). (c) Evolution of the valence fraction contribution of the measured spectra as a function of irradiation flux.

and  $V^{5+}$  states. After irradiation, the stoichiometric  $V^{3+}$  component is strongly enhanced. As seen in Fig. 3d, the  $V^{4+}$  contribution shows the largest change as a function of flux, whereas the  $V^{5+}$  component appears more robust to irradiation. The preminence of a  $V^{5+}$  oxidation state is consistent with the results in ref.,<sup>14</sup> where a major  $V^{5+}$  and a minor  $V^{4+}$  components were revealed by XPS on air-exposed  $VI_3$  crystals. The quantitative differences can be ascribed to the procedural standards applied in the two cases, mainly regarding the time of exposure, and the composition and background pressure of the atmospheric contaminants.

To evaluate the effect of X-ray irradiation when comparing clean and aged surfaces, we also carried out further XPS measurements of the V  $2p$  core level and the adjacent O  $1s$  peak, on as-cleaved, aged and irradiated samples (Fig. 4). Here, "irradiated" refers to the surface area that was exposed to the maximum X-ray flux and consequently displayed the changes in the XAS spectrum for a photon flux  $\approx 2.40 \times 10^{10}$  photons  $s^{-1}$  in Fig. 3. XPS peaks were fitted with multiplet peaks to disentangle the different contributions. This complementary analysis can be related to the XAS analysis to understand the relation between the valence, chemical state, and degree and type of contamination at the surface of the crystal.

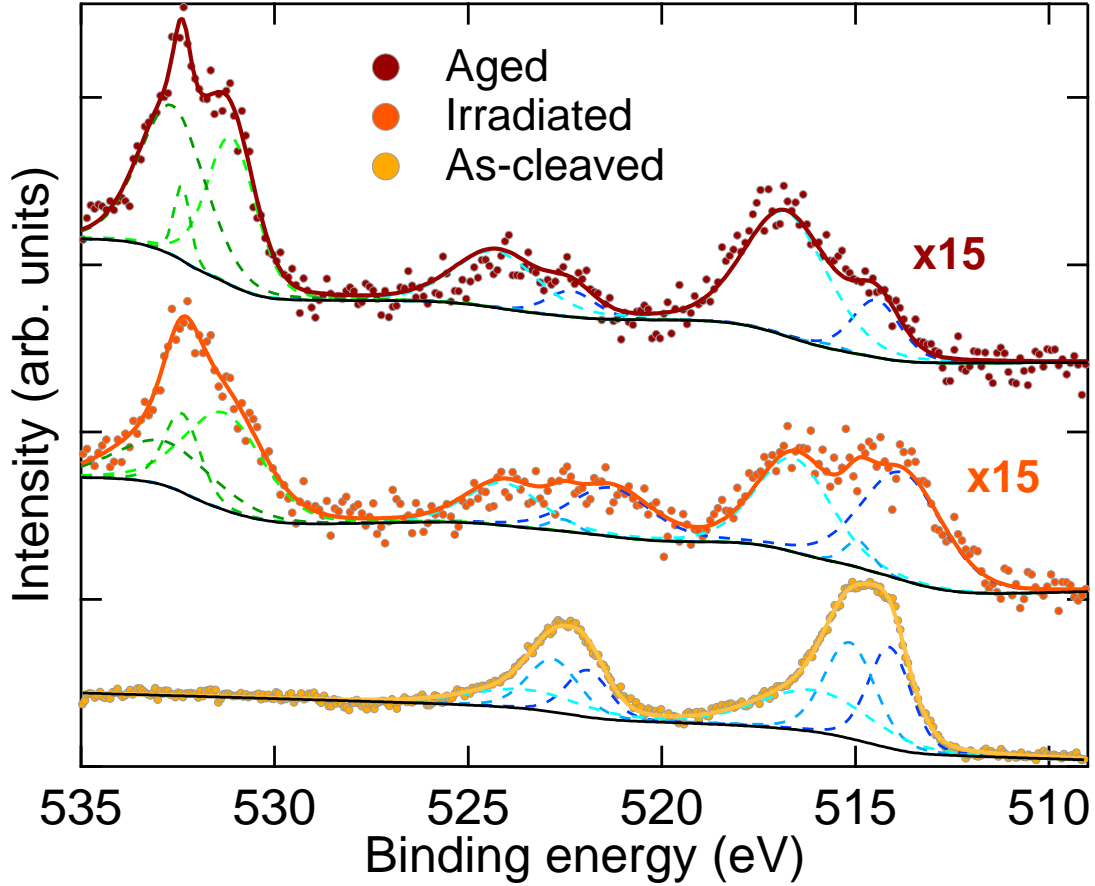


Figure 4: XPS spectra of as-cleaved, aged and irradiated samples; solid lines are fits of the experimental curves, dashed lines are the different components for V (blue/teal) and O (green) signals.

In the XPS spectra, we can see how the aged sample shows the majority of the V  $2p$  signal coming from higher binding energies compared to the as-cleaved one. After irradiation, the component at lower binding energies has emerged, consistently with what seen in XAS (Fig. 3c). The O  $1s$  peak contains several components, corresponding to different bound states. At the lowest binding energy, the O signal marks the presence of vanadium- $O^{2-}$  bonds; the higher binding energy component can be likely ascribed to surface bonded  $H_2O$  replacing the  $I^-$  ligands,<sup>14,29,30</sup> with possibly a minor contribution from O-C bonds.<sup>31</sup> The element ratio O:V in mol% can be approximately estimated as 1.7:1 in the aged sample, and 1.3:1 in the irradiated sample, by combining the photoionization cross sections and the respective integrated areas. It has to be underlined that this rough estimation does not



take into account the different distribution of the two atomic species within the probed thickness. Given that XAS, a more depth-sensitive technique, also reveals chemical changes upon irradiation, we consider reasonable the assumption that, within the probing depth of XPS at these photon energies (around 1 nm<sup>32</sup>), both O and V are evenly distributed in the sample. The overall O 1s signal in Fig. 4 decreases by roughly 25 % after irradiation; within the multiplet structure, the peak at highest binding energies is more strongly suppressed, whereas the peak at lower binding energies decreases less dramatically and considerably broadens. Conversely, the integrated areas of the V 2p structures do not change within the level of confidence of the fit. Compared to the expectations for compounds displaying 4+ or 5+ valence, the relatively low O:V ratio accounts also for the presence of clean VI<sub>3</sub>, whose fraction at low binding energies indeed becomes larger after irradiation.

From these observations we can surmise that the impinging X-rays at mild photon flux intensities partially desorb oxygen and H<sub>2</sub>O molecules hydrating VI<sub>3</sub>, and change the coordination and bonding of the vanadium oxides.

We also consider that, in principle, we cannot exclude also the formation of 3+ valence oxides giving rise to the increase of the V 2p signal at low binding energies in the aged and irradiated samples. However, the appearance of pre-edge features at V *L*<sub>3</sub> edge of XAS spectra after high flux exposure (see Fig. 3c) suggests the partial recovery of stoichiometric pristine VI<sub>3</sub>. In addition, given the likely high degree of surface disorder and the consequent lower statistics in the acquired spectra, assigning several multiplet peaks as in the as-cleaved sample is a much more challenging task for the aged and irradiated cases. In any case, the as-cleaved sample itself shows a nontrivial multiplet structure, which cannot be fitted by a single 2p doublet. The lack of a well-defined XPS peak suggests that the electronic state of VI<sub>3</sub> might be more complicated to understand than a simple V<sup>3+</sup> state. For example, Mastrippolito *et al.* have suggested that even pristine VI<sub>3</sub> intrinsically hosts trapped electrons giving rise to V<sup>2+</sup> localized states.<sup>33</sup> Moreover, there is a growing consensus that a mixed-orbital state characterized by strong covalency of the metal-ligand bond is instrumental in

correctly describing the electronic and magnetic properties of transition metal halides,<sup>20,34,35</sup> making the interpretation of XPS spectra more challenging.

## Conclusions

In this study, we combined X-ray absorption and X-ray photoemission spectroscopies to investigate the chemical stability of freshly cleaved  $\text{VI}_3$  single crystals. We observed how surface degradation induced by the interaction of the hygroscopic surface with spurious oxygen and water molecules, even in UHV conditions, leads to chemical alteration of the first monolayers, with the formation of vanadates. Surface stoichiometry, however, is at least partially recovered by soft X-ray irradiation under mild photon fluxes.

These results provide experimental evidence of the relatively weak interaction between the aged superficial layers and the stoichiometric underlayer, which can be removed by low energy means from the preserved part of the crystal.

## Acknowledgments

A.D.V. acknowledges financial support from the Max Planck Society and BERLIN QUANTUM, an initiative endowed by the Innovation Promotion Fund of the city of Berlin. We thank A. Fondacaro for the support in devising and commissioning the glovebox-UHV handling and transfer system. This work was performed in the framework of the NFFA-SPRINT facility, supported by MUR as the Activity of International Relevance NFFA ([www.trieste.NFFA.eu](http://www.trieste.NFFA.eu)). G.P. acknowledges financial support from PNRR MUR project PE0000023-NQSTI. We thank G. Fratesi and S. Achilli for fruitful discussion.

## Author Contributions

A.D.V. and G.P. conceived the research project. A.D.V., V.P., and G.V. performed the synchrotron measurements. A.D.V. analyzed the data under the supervision of G.V. A.D.V. and G.V. wrote the manuscript, with contributions from all authors.

## References

- (1) Gibertini, M.; Koperski, M.; Morpurgo, A.; Novoselov, K. Magnetic 2D materials and heterostructures. *Nat. Nanotechnol.* **2019**, *14*, 408–419.
- (2) Kajale, S.; Hanna, J.; Jang, K.; Sarkar, D. Two-dimensional magnetic materials for spintronic applications. *Nano Res* **2024**, *17*, 743–762.
- (3) Huang, B.; Clark, G.; Navarro-Moratalla, E.; Klein, D.; Cheng, R.; Seyler, K.; Zhong, D.; Schmidgall, E.; McGuire, M.; Cobden, D.; Yao, W.; Xiao, D.; Jarillo-Herrero, P.; Xu, X. Layer-dependent ferromagnetism in a van der Waals crystal down to the monolayer limit. *Nature* **2017**, *546*, 270–273.
- (4) Jiang, S.; Shan, J.; Mak, K. Electric-field switching of two-dimensional van der Waals magnets. *Nature Mater* **2018**, *17*, 406–410.
- (5) Jiang, S.; Li, L.; Wang, Z.; Mak, K.; Shan, J. Controlling magnetism in 2D CrI<sub>3</sub> by electrostatic doping. *Nature Nanotech* **2018**, *13*, 549–553.
- (6) Huang, B.; Clark, G.; Klein, D.; MacNeill, D.; Navarro-Moratalla, E.; Seyler, K.; Wilson, N.; McGuire, M.; Cobden, D.; Xiao, D.; Yao, W.; Jarillo-Herrero, P.; Xu, X. Electrical control of 2D magnetism in bilayer CrI<sub>3</sub>. *Nature Nanotech* **2018**, *13*, 544–548.
- (7) Zhang, X.; Wang, L.; Su, H.; Xia, X.; Liu, C.; Lyu, B.; Lin, J.; Huang, M.; Cheng, Y.; Mei, J.-W.; Dai, J.-F. Strain Tunability of Perpendicular Magnetic Anisotropy in van der Waals Ferromagnets VI3. *Nano Lett.* **2022**, *22*, 9891–9899.

- (8) Soriano, D.; Katsnelson, M.; Fernández-Rossier, J. Magnetic Two-Dimensional Chromium Trihalides: A Theoretical Perspective. *Nano Lett.* **2020**, *9*, 6225–6234.
- (9) Lin, Z.; Huang, B.; Hwangbo, K.; Jiang Q. and Zhang, Z., Q. Liu; Fei, Z.; Lv, H.; Millis, A.; McGuire, M.; Xiao, D.; Chu, J.-H.; Xu, X. Magnetism and Its Structural Coupling Effects in 2D Ising Ferromagnetic Insulator  $\text{VI}_3$ . *Nano Lett.* **2021**, *21*, 9180–9186.
- (10) De Vita, A.; Sant, R.; Polewczyk, V.; van der Laan, G.; Brookes, T., N.B. Kong; Cava, R.; Rossi, G.; Vinai, G.; Panaccione, G. Evidence of Temperature-Dependent Interplay between Spin and Orbital Moment in van der Waals Ferromagnet  $\text{VI}_3$ . *Nano Lett.* **2024**, *24*, 1487–1493.
- (11) Hao, Y.; Gu, Y.; Gu, Y.; Feng, E.; Cao, H.; Chi, S.; Wu, H.; Zhao, J. Magnetic Order and Its Interplay with Structure Phase Transition in van der Waals Ferromagnet  $\text{VI}_3$ . *Chinese Physics Letters* **2021**, *38*, 096101.
- (12) Hovančík, D.; Pospíšil, J.; Carva, K.; Sechovský, V.; Piamonteze, C. Large Orbital Magnetic Moment in  $\text{VI}_3$ . *Nano Lett.* **2023**, *23*, 1175–1180.
- (13) Kratochvílová, M.; Uhlířová, K.; Míšek, M.; Holý, V.; Zázvorka, J.; Veis, M.; Pospíšil, J.; Son, S.; Park, J.-G.; Sechovský, V. The surface degradation and its impact on the magnetic properties of bulk  $\text{VI}_3$ . *Materials Chemistry and Physics* **2022**, *278*, 125590.
- (14) Mastrippolito, D.; Swiatek, H.; Moras, P.; Jugovac, M.; Gunnella, R.; Lozzi, L.; Benassi, P.; Klimczuk, T.; Ottaviano, L. Intense and stable room-temperature photoluminescence from nanoporous vanadium oxide formed by in-ambient degradation of  $\text{VI}_3$  crystals. *Journal of Luminescence* **2022**, *251*, 119137.
- (15) Wang, W.; Sun, R.; Shen, W.; Jia, Z.; Deepak, F. L.; Zhang, Y.; Wang, Z. Atomic structure and large magnetic anisotropy in air-sensitive layered ferromagnetic  $\text{VI}_3$ . *Nanoscale* **2023**, *15*, 4628–4635.

- (16) Shcherbakov, D.; Stepanov, P.; Weber, D.; Wang, Y.; Hu, J.; Zhu, Y.; Watanabe, K.; Taniguchi, T.; Mao, W., Z. Windl; Goldberger, J.; Bockrath, M.; Ning Lau, C. Raman Spectroscopy, Photocatalytic Degradation, and Stabilization of Atomically Thin Chromium Tri-iodide. *Nano Lett.* **2018**, *18*, 4214–4219.
- (17) Paolucci, V.; Mastrippolito, D.; Ricci, V.; Świątek, H.; Klimczuk, T.; Ottaviano, L.; Cantalini, C. Two-Dimensional  $\text{CrCl}_3$ -Layered Trihalide Nanoflake Sensor for the Detection of Humidity,  $\text{NO}_2$ , and  $\text{H}_2$ . *ACS Appl. Nano Mater.* **2024**, *7*, 3679–3690.
- (18) Panaccione, G. et al. Advanced photoelectric effect experiment beamline at Elettra: A surface science laboratory coupled with Synchrotron Radiation. *Review of Scientific Instruments* **2009**, *80*, 043105.
- (19) De Vita, A. et al. Influence of Orbital Character on the Ground State Electronic Properties in the van Der Waals Transition Metal Iodides  $\text{VI}_3$  and  $\text{CrI}_3$ . *Nano Lett.* **2022**, *22*, 7034–7041.
- (20) Sant, R.; De Vita, A.; Polewczyk, V.; Pierantozzi, G.; Mazzola, F.; Vinai, G.; van der Laan, G.; Panaccione, G.; Brookes, N. Anisotropic hybridization probed by polarization dependent x-ray absorption spectroscopy in  $\text{VI}_3$  van der Waals Mott ferromagnet. *Journal of Physics: Condensed Matter* **2023**, *35*, 405601.
- (21) Abbate, M.; Pen, H.; Czyżyk, M.; de Groot, F.; Fuggle, J.; Ma, Y.; Chen, C.; Sette, F.; Fujimori, A.; Ueda, Y.; Kosuge, K. Soft X-ray absorption spectroscopy of vanadium oxides. *Journal of Electron Spectroscopy and Related Phenomena* **1993**, *62*, 185–195.
- (22) Zimmermann, R.; Claessen, R.; Reinert, F.; Steiner, P.; Hüfner, S. Strong hybridization in vanadium oxides: evidence from photoemission and absorption spectroscopy. *Journal of Physics: Condensed Matter* **1998**, *10*, 5697.
- (23) Wu, M.; Zheng, J.-C.; Wang, H.-Q. Investigation of the vanadium  $L_{23}$ -edge x-ray ab-

- sorption spectrum of  $\text{SrVO}_3$  using configuration interaction calculations: Multiplet, valence, and crystal-field effects. *Phys. Rev. B* **2018**, *97*, 245138.
- (24) Polewczyk, V.; Chaluvadi, S.; Dagur, D.; Mazzola, F.; Punathum Chalil, S.; Petrov, A.; Fujii, J.; Panaccione, G.; Rossi, G.; Orgiani, P.; Vinai, G.; Torelli, P. Chemical, structural and electronic properties of ultrathin  $\text{V}_2\text{O}_3$  films on  $\text{Al}_2\text{O}_3$  substrate: Implications in Mott-like transitions. *Applied Surface Science* **2023**, *610*, 155462.
- (25) Frazer, B. H.; Gilbert, B.; Sonderegger, B. R.; De Stasio, G. The probing depth of total electron yield in the sub-keV range: TEY-XAS and X-PEEM. *Surface Science* **2003**, *537*, 161–167.
- (26) Tian, S.; Zhang, J.-F.; Li, C.; Ying, T.; Li, S.; Zhang, X.; Liu, K.; Lei, H. Ferromagnetic van der Waals Crystal  $\text{VI}_3$ . *Journal of the American Chemical Society* **2019**, *141*, 5326–5333.
- (27) Vinai, G.; Bigi, C.; Rajan, A.; Watson, M. D.; Lee, T.-L.; Mazzola, F.; Modesti, S.; Barua, S.; Ciomaga Hatnean, M.; Balakrishnan, G.; King, P. D. C.; Torelli, P.; Rossi, G.; Panaccione, G. Proximity-induced ferromagnetism and chemical reactivity in few-layer  $\text{VSe}_2$  heterostructures. *Phys. Rev. B* **2020**, *101*, 035404.
- (28) Polewczyk, V.; Mezhoud, M.; Rath, M.; El-Khaloufi, O.; Bassato, F.; Fouchet, A.; Prellier, W.; Frégnaux, M.; Aureau, D.; Braglia, L.; Vinai, G.; Torelli, P.; Lüders, U. Formation and Etching of the Insulating Sr-Rich  $\text{V}^{5+}$  Phase at the Metallic  $\text{SrVO}_3$  Surface Revealed by Operando XAS Spectroscopy Characterizations. *Advanced Functional Materials* **2023**, *33*, 2301056.
- (29) Linn, J.; Swartz, W. An XPS study of the water adsorption/desorption characteristics of transition metal oxide surfaces: Microelectronic implications. *Applications of Surface Science* **1984**, *20*, 154–166.

- (30) Choudhury, T.; Saied, S. O.; Sullivan, J. L.; Abbot, A. M. Reduction of oxides of iron, cobalt, titanium and niobium by low-energy ion bombardment. *Journal of Physics D: Applied Physics* **1989**, *22*, 1185.
- (31) Ren, Q.; Qin, N.; Liu, B.; Yao, Y.; Zhao, X.; Deng, Z.; Li, Y.; Dong, Y.; Qian, D.; Su, B.-L.; Zhang, W.; Wang, H.-E. An oxygen-deficient vanadium oxide@N-doped carbon heterostructure for sodium-ion batteries: insights into the charge storage mechanism and enhanced reaction kinetics. *J. Mater. Chem. A* **2020**, *8*, 3450–3458.
- (32) Seah, M. P.; Dench, W. A. Quantitative electron spectroscopy of surfaces: A standard data base for electron inelastic mean free paths in solids. *Surface and Interface Analysis* **1979**, *1*, 2–11.
- (33) Mastrippolito, D.; Camerano, L.; Świątek, H.; Šmíd, B. c. v.; Klimczuk, T.; Ottaviano, L.; Profeta, G. Polaronic and Mott insulating phase of layered magnetic vanadium trihalide  $VCl_3$ . *Phys. Rev. B* **2023**, *108*, 045126.
- (34) He, W.; Sears, J.; Barantani, F.; Kim, T.; Villanova, J. W.; Berlijn, T.; Lajer, M.; McGuire, M. A.; Pellicciari, J.; Bisogni, V.; Johnston, S.; Baldini, E.; Mitrano, M.; Dean, M. P. M. Dispersive Dark Excitons in van der Waals Ferromagnet  $CrI_3$ . *Phys. Rev. X* **2025**, *15*, 011042.
- (35) De Vita, A.; Stavrić, S.; Sant, R.; Brookes, N. B.; Vobornik, I.; Panaccione, G.; Piccozzi, S.; Wolf, M.; Rettig, L.; Ernstorfer, R.; Pincelli, T. Orbital mixing as key ingredient for magnetic order in a van der Waals ferromagnet. 2025; <https://arxiv.org/abs/2507.04144>.

# Supporting Information - Surface restoration in hygroscopic $\text{VI}_3$ crystals via synchrotron soft X-ray irradiation

A. De Vita,<sup>1,2,\*</sup> V. Polewczyk,<sup>3</sup> G. Panaccione,<sup>4</sup> and G. Vinai<sup>4,†</sup>

<sup>1</sup>*Institut für Physik und Astronomie,*

*Technische Universität Berlin,*

*Strasse des 17 Juni 135, 10623 Berlin, Germany*

<sup>2</sup>*Fritz Haber Institute of the Max Planck Society, Faradayweg 4–6, 14195 Berlin, Germany*

<sup>3</sup>*Université Paris-Saclay, UVSQ, CNRS,*

*GEMaC, 78000, Versailles, France*

<sup>4</sup>*CNR - Istituto Officina dei Materiali (IOM), S.S. 14, km 163.5, 34149 Trieste, Italy*



## ADDITIONAL FIGURES

For completeness, we present in Fig. S1 the XPS survey at 800 eV acquired on pristine, clean  $\text{VI}_3$  right after cleaving, after four hours, and after eight hours. The photon flux was quantified as  $0.28 \text{ photons s}^{-1}$ . We do not find any evidence of degradation or modifications of the core levels.

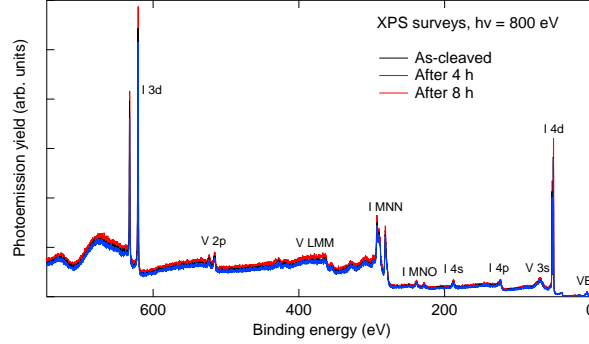


FIG. S1. XPS surveys acquired at 100 K with 800 eV photons.

In Fig. S2 we show the effect of irradiation on the measured spot compared to other areas on the sample surface. In Fig. S2a, the 2D map of the sample displays three spots (A, B, and C) where data have been acquired. Spot A has been irradiated with the maximum photon flux ( $2.8 \times 10^9 \text{ photons s}^{-1}$ , Fig. 3a of the main text), spot B and C are pristine. Fig. S2b collects the XAS spectra across the V  $L_{2,3}$  edges in each of the three spots – the top and bottom curves (A-1 and A-2) have both been performed on A, respectively before and after the acquisition of the spectra B and C. The photon flux was  $2.8 \times 10^9 \text{ photons s}^{-1}$ . It is clear from the lineshape and the position of the main peaks that, after exposure to the maximum flux, the irradiated spot is characterized by a different chemical state with respect to the other areas of the sample, and that such effect is not transiently appearing under the beam.

\* alessandro.de.vita@tu-berlin.de

† vinai@iom.cnr.it

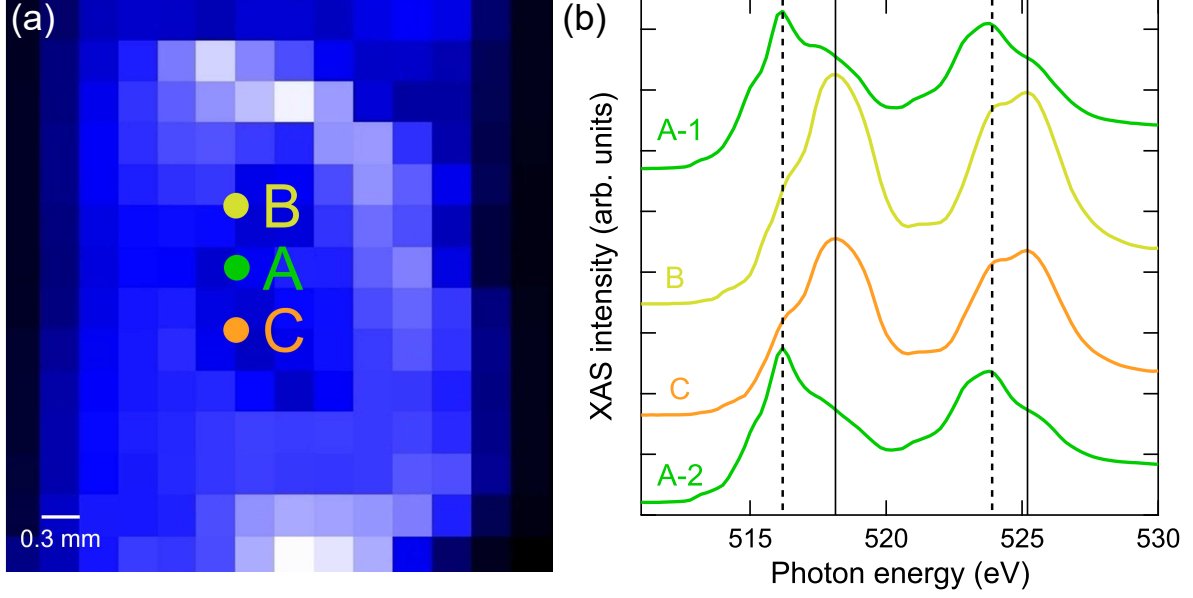


FIG. S2. (a) 2D map of the sample holder area; the color scale is the TEY signal (lighter corresponds to higher signal intensity). The bright pixels indicate the edges of the sample. (b) XAS spectra across the V  $L_{2,3}$  edges for a photon flux  $2.8 \times 10^9$  photons  $s^{-1}$ ; the colors correspond to the spots in (a) where the spectrum was measured. The labels A-1 and A-2 refer both to spectra measured on A at different times, as explained in the main text. The dashed and solid lines highlight the main  $L_3$  and  $L_2$  peaks for the irradiated and aged surfaces, respectively.